

Air stable electron-transporting and ambipolar bay substituted perylene bisimides

Renji R. Reghu,^a Hari Krishna Bisoyi,^a Juozas V. Grazulevicius,^{*a} Padmesh Anjukandi,^b Valentas Gaidelis^c and Vygintas Jankauskas^c

Received 13th March 2011, Accepted 23rd March 2011

DOI: 10.1039/c1jm11091h

Four new perylene bisimides containing carbazolyl and triphenylamino electron-donor groups in the bay region have been designed, synthesized and characterized. The materials possess high thermal stability and form uniform films. They display a wide absorption window extending to the near infrared region of the spectrum and demonstrate efficient photoinduced intramolecular electron transfer. Ionization potential values of these perylene bisimide derivatives measured by photoelectron spectroscopy range from 5.8 eV to 6 eV. Charge-transporting properties were investigated by the xerographic time of flight (XTOF) technique. Complementary ambipolar charge-transport was observed in differently linked carbazolyl substituted perylene bisimides while the triphenylamino substituted material exhibited competent electron drift mobility ($>10^{-3}$ cm² V⁻¹ cm⁻¹) under ambient conditions. Density functional theory (DFT) calculations were performed for carbazolyl bay substituted perylene bisimides in order to understand the complementary ambipolar charge transport as well as the difference in the optical properties.

1. Introduction

Recently there has been an unprecedented growth of interest in organic semiconductors *i.e.* organic materials for application in electronic and optoelectronic devices such as light emitting diodes, photovoltaic devices and field-effect transistors *etc.*^{1–5} The superiority of organic semiconductors over their inorganic counterparts resides in their tremendous architectural flexibility, inexpensiveness and ease of processing and device fabrication. However, one of the major challenges in the field is the development of high-mobility and stable electron-transporting (n-type) organic semiconductors for thin film device structures to complement the high efficiency of current generation p-type materials which would enable durable devices with high operating speeds and lower power consumption.^{6–8} The disadvantageous low charge carrier mobility in most of the known n-type materials at ambient conditions is mainly due to the trapping of charge carriers (*i.e.*, electrons) by common atmospheric oxidants such as oxygen, water *etc.*^{9,10} In this context, appropriate molecular design towards efficient charge transport seems to be the first stepping stone.^{11,12}

Perylene bisimide derivatives form a class of interesting n-type organic semiconductors owing to excellent charge carrier transport in conjunction with their outstanding chemical, thermal and photochemical stability.^{13–16} Very high electron mobility of perylene bisimide derivatives has qualified them to be widely employed in electronic and optoelectronic devices.^{6–8} Accordingly numerous perylene bisimide derivatives carrying different substituents on the imide positions as well as on the carbocyclic core, the so-called bay region, have been synthesized and investigated.^{13–16} However stable ambipolar molecular materials based on π -conjugated perylene bisimides have not been explored well and are still interesting in the perspective of cost effective single layer organic light emitting diodes and field-effect transistors.^{17–20} On the other hand, redox-active carbazole and triphenylamine derivatives are well known hole-transporting materials and have been exploited extensively for various optoelectronic applications.^{21–24} Additionally carbazole derivatives possess excellent photorefractive properties while triphenylamines act as organic photoconductors in the xerographic industry.^{21–24} It is interesting to note that the optoelectronic devices fabricated from electroactive materials derived from 2,7-substituted carbazoles exhibit better performances than 3,6-substituted carbazole derivatives.^{25–27} Moreover, molecular materials based on 2-substituted carbazolyl derivatives have been less extensively studied because of the much easier synthetic protocol of its regioisomeric counterpart; *i.e.* 3-substituted carbazoles. To the best of our knowledge, the donor–acceptor hybrids combining perylene bisimides and carbazoles at the bay region are hitherto unknown.

^aDepartment of Organic Technology, Kaunas University of Technology, Radvilenu pl. 19, LT-50254 Kaunas, Lithuania. E-mail: juozas.grazulevicius@ktu.lt; Fax: +37037 300152; Tel: +37037 300193

^bInstitute of Fundamental Sciences, Massey University, Palmerston North, New Zealand

^cDepartment of Solid State Electronics, Vilnius University, Sauletekio al. 9, LT-10222 Vilnius, Lithuania

Furthermore, the combination of hole-transporting and electron-donating planar carbazole and non-planar triphenylamine derivatives with electron-transporting perylene bisimides at molecular level may lead to novel multichromophoric donor-acceptor molecular materials with interesting and useful optical and charge-transporting properties important for various device applications. Keeping this in mind we have designed and synthesized new 1,7-bay substituted perylene bisimide derivatives directly linked to electron-donating triphenylamino and different carbazolyl moieties furnishing efficient electron-transporting and ambipolar materials possessing excellent photoinduced charge transfer properties. Herein we present the thermal, optical, photophysical, electrochemical and photoelectrical characterizations and preliminary quantum chemical calculations of the newly synthesized molecular materials based on bay substituted perylene bisimides.

2. Results and discussion

2.1. Synthesis

The chemical structures of the newly designed target materials are shown in Fig. 1. 1,7-Bis[4-(diphenylamino)phenyl] *N,N'*-2-ethylhexyl perylene bisimide (**1**) was synthesised by the Suzuki-Miyaura coupling reaction of 1,7-dibromoperylene bisimide with 4-(diphenylamino)phenylboronic acid (**4-DPB**). Other compounds, 1,7-bis(9-ethyl-2-carbazolyl) *N,N'*-2-ethylhexyl perylene bisimide (**2**), 1,7-bis(9-ethyl-3-carbazolyl) *N,N'*-2-ethylhexyl perylene bisimide (**3**) and 1,7-bis(9-ethyl-3-carbazolyl) *N,N'*-dodecyl perylene bisimide (**4**) were also synthesized by the Suzuki-Miyaura coupling between 1,7-dibromoperylene bisimide and the corresponding mono boronic acid pinacol ester derivatives of carbazole (Scheme 1). 1,7-Dibromo *N,N'*-2-ethylhexyl perylene bisimide (**5**) and 1,7-dibromo *N,N'*-dodecyl perylene bisimide (**6**) were in turn prepared by the bromination of commercially available 3,4,9,10-perylene tetracarboxylic dianhydride followed by the condensation with corresponding alkyl amines, 2-ethylhexylamine and *n*-dodecylamine, respectively. 9-Ethyl-2-carbazolyl boronic acid pinacol ester (**2-CZ**) was obtained from 4-bromobiphenyl by nitration followed by ring closure with triphenylphosphine and the consequent *N*-alkylation and borylation using 2-isopropoxy-4,4,5,5-tetramethyl-1,3,2-dioxaborolane.^{28–30} The precursor for compounds **3** and **4**, 9-ethyl-3-carbazolyl boronic acid pinacol ester (**3-CZ**), was prepared from 3-bromocarbazole by *N*-alkylation and

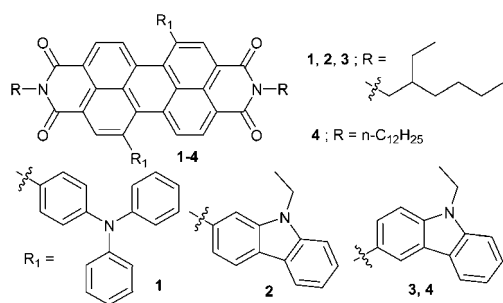
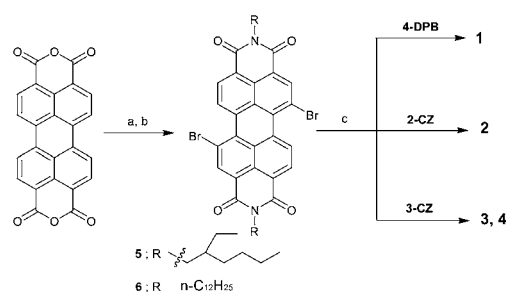


Fig. 1 Chemical structures of compounds 1–4.



Scheme 1 Synthetic route for the preparation of compounds 1–4. *Reagents and conditions:* (a) Br₂, conc. H₂SO₄/I₂, 80 °C, 24 h; (b) dodecylamine or 2-ethylhexylamine, CH₃COOH/*N*-methylpyrrolidone, 120 °C, 12 h; (c) Pd(Ph₃)₂Cl₂, KOH, THF–H₂O, 80 °C, 8–12 h.

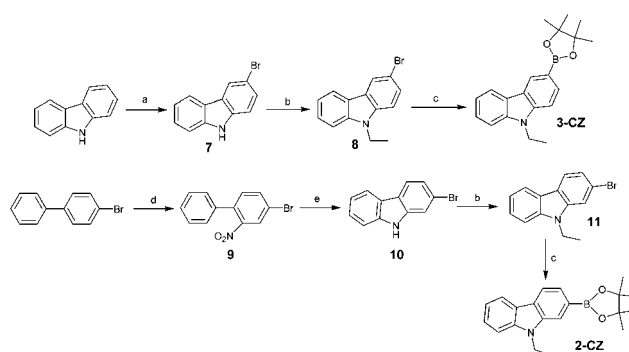
subsequent borylation as reported elsewhere.^{31,32} The synthesis of key boronic acid pinacol esters is described in Scheme 2.

The synthesized compounds were purified by column chromatography and characterized by ¹H NMR, ¹³C NMR, MALDI-TOF, IR spectroscopy and elemental analysis. The spectral and elemental analysis data are in good agreement with their chemical structures.

2.2. Thermal characteristics

The glass transition temperatures (*T_g*) of the synthesized perylene bisimide derivatives are summarised in Table 1. They range from 81 °C to 95 °C. The linking topology of perylene bisimide and carbazole derivatives seems not to have any substantial influence on their *T_g*. *T_g* of 2-carbazolyl substituted derivative (**2**) is comparable to that of its 3-carbazolyl substituted isomer (**3**). The effect of the branched but shorter alkyl chain and longer but linear alkyl chain on the glass transition of 3-carbazolyl substituted derivatives is also comparable. *T_g* of **3** is close to that of **4**.

Thermal stability of compounds 1–4 was estimated by thermogravimetric analysis (TGA). All the derivatives demonstrate high thermal stability. The temperatures of the onsets of thermal decomposition (*T_{ID}*) of perylene bisimide derivatives are collected in Table 1. They range from 438 °C to 471 °C. The *T_{ID}*



Scheme 2 Synthetic route for the preparation of carbazolyl boronic acid pinacol esters (**2-CZ** and **3-CZ**). *Reagents and conditions:* (a) Br₂, pyridine, 0 °C, 2 h; (b) C₂H₅I, KOH, DMF, RT, 24 h; (c) *n*-BuLi, 2-isopropoxy-4,4,5,5-tetramethyl-1,3,2-dioxaborolane, THF, –78 °C to RT, 12 h; (d) CH₃COOH/HNO₃, reflux, 5 h; (e) PPh₃, *ortho*-dichlorobenzene, 180 °C, 12 h.

Table 1 Thermal characteristics of 1–4^a

Compound	$T_g/^\circ\text{C}$	$T_m/^\circ\text{C}$	$T_{cr}/^\circ\text{C}$	$T_{ID}/^\circ\text{C}$
1	95	251	194	455
2	82	—	—	441
3	81	—	—	438
4	82	—	—	471

^a T_g – Glass transition temperature, T_m – Melting transition, T_{cr} – Crystallization temperature, T_{ID} – Thermal decomposition onset.

values of compounds 1–3 are comparable irrespective of the bay substituents. The difference in the T_{ID} values of 3 and 4 is pointing towards the influence of *N*-alkyl substituents on their thermal stability.

2.3. Optical and photoluminescent properties

The synthesized compounds are well soluble in common organic solvents like tetrahydrofuran, dichloromethane, chloroform *etc.*, facilitating their optical characterization in solution state. UV-Vis absorption spectra of dilute solutions are shown in Fig. 2. The wavelengths of absorption maxima are collected in Table 2. The low energy absorption edges of the newly synthesized compounds range from 669 nm to 787 nm and as anticipated for bay substitution by aromatic groups, are red shifted with respect to the unsubstituted parent compound, perylene bisimide (PBI), owing to their greater conjugation.^{33–35} Moreover, it is found that the least energy absorption band of 1 carrying triphenylamino moiety at the bay region is bathochromically shifted with respect to that of compounds 2–4 possessing carbazole units. This suggests distortion of the perylene core, known to occur upon bay substitution, to a lesser degree upon substitution by triphenylamino moiety as well as greater conjugation leading to relatively low optical band gap compared to those of carbazole derivatives.^{34,36} Furthermore, surprisingly the absorption bands of 3-carbazolyl substituted derivatives (3&4) are shifted both bathochromically and hyperchromically with respect to that of 2-carbazolyl substituted derivative (2), clearly indicating a different degree of perylene core distortion and/or different torsional angles of bay substituents in these topological isomers. Investigation of photoluminescent properties of 1–4 yields interesting

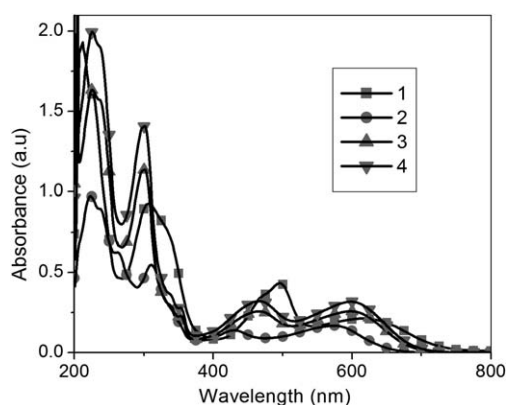


Fig. 2 UV-Vis absorption spectra of compounds 1–4 in THF (10^{-4} mol L^{-1}).

Table 2 Optical characterization data of 1–4^a

Compound	Absorption $\lambda_{\text{max}}/\text{nm}$	Emission $\lambda_{\text{max}}/\text{nm}$	$(\eta)^b$	$E_g^{\text{opt}}/\text{eV}^c$
1	211, 307, 496, 617	Non-fluorescent	—	1.58
2	224, 311, 430, 574	705	0.004	1.85
3	226, 301, 466, 599	756	0.03	1.74
4	226, 301, 466, 599	756	0.03	1.74

^a η – Fluorescence quantum yield. ^b Fluorescence was excited at 570 nm. ^c E_g^{opt} – Optical band gap. ^c Calculated from solution absorption edges.

results on the potential of these multichromophoric donor–acceptor hybrids. There is a complete self-quenching of the fluorescence of compound 1 whereas compounds 2–4 are almost non-fluorescent with trivial fluorescence quantum yields (Table 2). These results suggest that very efficient photo-induced intramolecular electron transfer occurs in these compounds. Since all these molecules absorb well in the visible–near IR region with efficient photo-induced intramolecular charge transfer, they can be promising candidates for application in photovoltaic devices.³⁷

2.4. Electrochemical properties

Electrochemical properties of selected compounds were studied by cyclic voltammetry in order to elucidate the electronic energy levels which determine the energy and electron transfer processes and the reversibility of redox processes.³⁸ Cyclic voltammograms of compounds 2 and 3 are given in Fig. 3. HOMO and LUMO energy levels of these compounds were calculated using ferrocene as the standard redox system.³⁹ The half wave potentials and HOMO–LUMO energy values are summarized in Table 3. Both the carbazolyl substituted perylene bisimides exhibit dianionic behaviour similar to other bay-substituted perylene derivatives.⁴⁰ Moreover they also undergo oxidation and display cationic behaviour which is believed to arise due to the influence of the electron donating carbazolyl bay-substituents. As can be seen from Table 3, compound 2 possesses higher electrochemical band gap than compound 3 and the trend is comparable with the optical band gaps. Relatively high LUMO levels of compounds 2 and 3 compared to other related materials may be attributed to the twisted structure and rather high electron density in the

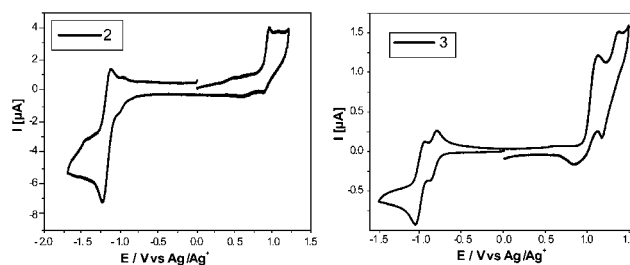


Fig. 3 Cyclic voltammograms of compounds 2 and 3. Electrolyte: $n\text{-Bu}_4\text{NPF}_6$ in DCM (0.01 mol L^{-1}). Working, counter and reference electrodes: glassy carbon, platinum wire and Ag/AgNO_3 (0.01 mol L^{-1} in acetonitrile) respectively. Scan rate: 100 mV s^{-1} .

Table 3 Electrochemical characteristics of compounds **2** and **3**^a

Compound	E_{red}/V	E_{oxi}/V	$E_{\text{red}}^{\text{onset}}/\text{V}$	$E_{\text{oxi}}^{\text{onset}}/\text{V}$	$E_{\text{HOMO}}/\text{eV}$	$E_{\text{LUMO}}/\text{eV}$	$E_{\text{g}}^{\text{ele}}/\text{eV}$
2	-1.13, -1.24; -0.94, -1.05	0.94, 0.87	-1.18; -0.97	0.90	-5.53	-3.66	1.87
3	-0.96, -1.05; -0.81, -0.87	1.37, 1.18; 1.12, 0.86	-1.05; -0.84	1.27; 0.99	-5.62	-3.79	1.83

^a $E_{\text{g}}^{\text{ele}}$ – Electrochemical band gap.

perylene core induced by bulky electron-donating bay substituents.^{40,41}

2.5. Photoelectrical properties

Ionization potentials (I_{p}) of solid layers of the synthesized compounds were measured by photoelectron spectroscopy (PES). Photoelectron spectra of **1–4** are given in Fig. 4. The intersection points of the linear parts of the spectra drawn with the abscissa axis give the ionization potential values. I_{p} values are rather close and range from 5.8 eV to 6.0 eV. The highest I_{p} value was observed for 2-carbazolyl substituted derivative (**2**). A small difference is observed in the values of HOMO (I_{p}) energy levels of carbazolyl derivatives (**2** and **3**) obtained by PES and electrochemical studies. This is due to the difference in molecular interactions and molecular arrangements in thin solid layers and in dilute solutions of these derivatives.

The xerographic time of flight (XTOF) technique was used for the evaluation of charge-transporting properties of thin layers of

compounds **1–4** in air. Compounds **1** and **2** provide good neat thin films. However, thin film preparation for XTOF experiment was not successful for **3** and therefore, a solid solution (1 : 1; wt.) was prepared with an inert polymer host, bisphenol Z-poly-carbonate (PC-Z). In order to have a fair comparison of charge-transporting properties in neat films between 2- and 3-carbazolyl substituted derivatives, compound **4** was synthesized and found to form good neat film.

All the compounds (**1–4**) exhibited capability of transporting both electrons and holes. This is evidenced by the practically equal amounts of positive and negative charges extracted after the impulse of strongly absorbed irradiation with the wavelength of 337 nm. However, due to the enhanced dispersivity of hole-transport we were not able to estimate the hole drift mobilities in the layer of **1**. XTOF charge drift mobility data for **1–4** are summarized in Table 4 and representative dU/dt transients for the neat films of **1** and **4** are shown in Fig. 5. A distinct inflection point indicating transit time with the sign of non-dispersive electron transport was observed in air for the neat film of **1** which was unaltered even after ambient storage for several weeks. Compound **2** also exhibited a non-dispersive electron transport with significantly high electron drift mobility whereas a dispersive and rather slow hole-transport was observed. For compounds **3** and **4**, charge-transport was dispersive; however, the drift mobility values were sufficiently high.

The room temperature electric field dependencies of hole and electron drift mobility (μ) values for the thin films of perylene bisimide derivatives **1**, **2** and **4** are given in Fig. 6. The linear dependencies of hole/electron-drift mobilities on the square root of electric field E are observed. In all cases charge drift mobility may be well approximated by the Poole–Frenkel relationship: $\mu = \mu_0 \exp(\alpha\sqrt{E})$, where α is the field dependence parameter and μ_0 is the zero field mobility obtained by extrapolating the linear dependencies to zero electric field.^{42,43} The highest electron mobility is observed for **1** containing triphenylamino moiety at the bay region and its value well exceeded $10^{-3} \text{ cm}^2 \text{ V}^{-1} \text{ s}^{-1}$ at high electric fields. Electron drift mobility values of **1** have also been

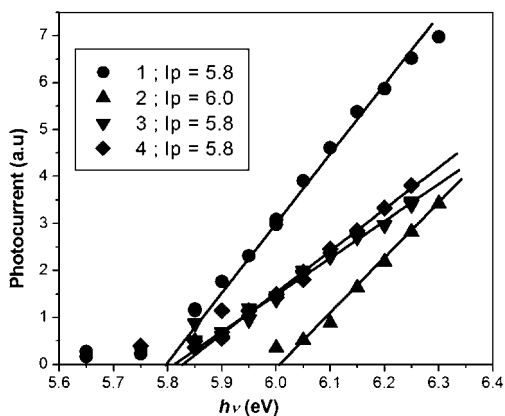


Fig. 4 Photoelectron spectra and ionization potentials (in eV) of the thin films of compounds **1–4**.

Table 4 XTOF charge mobility data of **1–4**^a

Compound	Electrons			Holes		
	μ_0	μ	α	μ_0	μ	α
1	2.8×10^{-4}	2.3×10^{-3}	0.0021	—	—	—
2	9.2×10^{-5}	1.4×10^{-3}	0.0027	8.1×10^{-11}	1.2×10^{-7}	0.007
^b 3	1.4×10^{-8}	1.2×10^{-6}	0.0045	1.2×10^{-7}	9.2×10^{-6}	0.0044
4	7.3×10^{-7}	8.9×10^{-5}	0.0021	5.8×10^{-5}	1.7×10^{-3}	0.0034

^a Zero-field mobilities (μ_0) in $\text{cm}^2 \text{ V}^{-1} \text{ s}^{-1}$, mobilities (μ) at an electric field of 10^6 V cm^{-1} in $\text{cm}^2 \text{ V}^{-1} \text{ s}^{-1}$ and field dependences (α) in $(\text{cm V}^{-1})^{1/2}$ of holes and electrons in solid layers. ^b Solid solution [(**3** + PC-Z) 1 : 1; wt.].

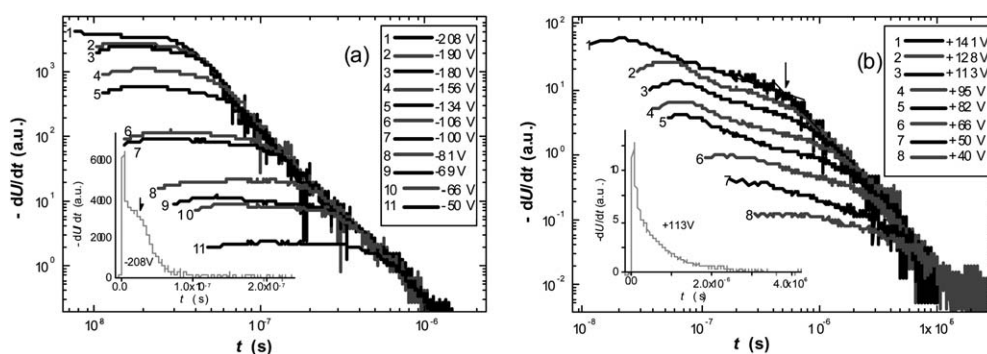


Fig. 5 XTOF transients for the neat films of perylene derivatives **1** (a) and **4** (b). 1 ns laser operating at 337 nm was used, $T = 25^\circ\text{C}$. Arrows on insets (a) and on main layout (b) indicate transit time of electrons and holes respectively at corresponding surface voltages.

measured after several weeks in order to evaluate the charge-transporting stability in ambient conditions and it was found that they are almost insensitive to ambient storage. The combination of efficient charge carrier mobility and its ambient stability renders **1** particularly attractive for the fabrication of field effect transistors.^{11,12} Compounds **3** and **4** exhibit a similar pattern of ambipolar charge transportation. However, the magnitude of carrier mobility in the layer of compound **3** is less compared to that of **4** and it may be due to the less amount of chromophores in the solid solution layer of **3** (Table 4). It is interesting to compare the electron and hole drift mobilities in compounds **2** and **4** since they exhibit reverse trends in charge transportation. Compound **2**, in which carbazolyl groups are linked to perylene bay *via* their 2-position, exhibits a higher order of electron mobility ($>10^{-3} \text{ cm}^2 \text{ V}^{-1} \text{ s}^{-1}$) than **4** ($>10^{-5} \text{ cm}^2 \text{ V}^{-1} \text{ s}^{-1}$). However compound **4**, in which carbazolyl groups are linked to perylene bay *via* their 3-position, displays a higher order of hole mobility ($>10^{-3} \text{ cm}^2 \text{ V}^{-1} \text{ s}^{-1}$) than **2** ($>10^{-7} \text{ cm}^2 \text{ V}^{-1} \text{ s}^{-1}$). It should be noted that **2** and **4** differ in the position of covalent linking of carbazolyl groups to the perylene bisimide core. Therefore the observation of these complementary charge carrier mobilities just by changing the linking topology of the carbazolyl groups to the perylene core is quite remarkable.

2.6. DFT calculations

Quantum chemistry studies were performed for carbazolyl-substituted perylene bisimides **2** and **3** in order to acquire a deeper insight into their frontier molecular orbitals (FMOs),

band-gap energies, twisting of the perylene core (dihedral angle, α) and that of the bay substituted carbazoles with respect to the perylene core (torsional angle, β_1 and β_2), in accordance with the previous works.^{33,44} DFT calculations were as implemented in the *Gamess US* package.⁴⁵ Perylene bisimide derivatives were first geometry optimised using a semi-empirical PM6 basis set as implemented in *MOPAC*⁴⁶ and these PM6 optimized geometries were further subjected to complete geometry optimization using DFT calculations at the basis B3LYP/6-311G*. These optimized structures were then used to perform single point energy calculations at B3LYP/6-311++G** basis to analyse the above mentioned properties.

Fig. 7 (A & B) demonstrates the calculated frontier orbitals for molecules **2** and **3**. HOMO and LUMO energy levels of these molecules established by quantum chemical calculations are summarised in Table 5. As seen earlier with the perylenes, these molecules behave in a similar way with their LUMO mainly localised on the perylene bisimide core.⁴⁴ However, there is a considerable difference observed between the HOMO orbitals of species **2** and **3**. In compound **3**, it is seen that the HOMO is distributed evenly on the perylene ring as well as on both the carbazole units. However in **2**, the HOMO is more localised on one of the carbazole units unlike in **3**. Fig. 7(C) demonstrates the FMO for molecule **2** at two different isosurface values; (a) [same as in 7(A)] and (b). It clearly shows the HOMO being spanned throughout the molecule; but not evenly like in **3** and centred mainly on one of the carbazoles. Thus it is evident that the carbazole substitutions enhance a considerable difference in the HOMO orbitals of **2** and **3**, when there is a difference in their

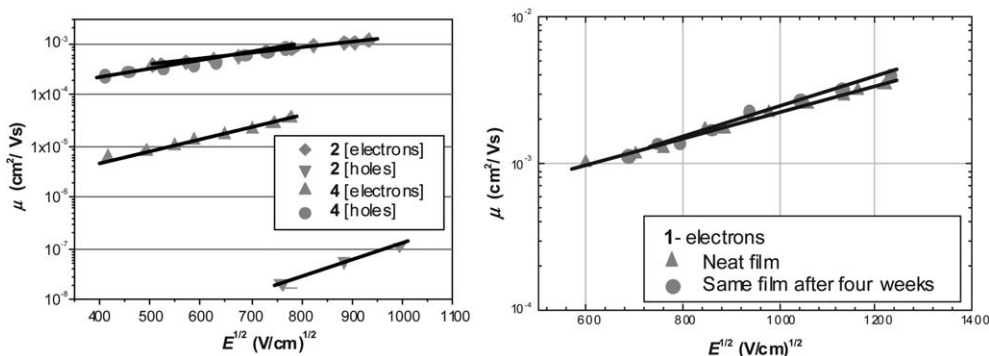


Fig. 6 The electric field dependencies of charge mobilities of **1**, **2** and **4** in air.

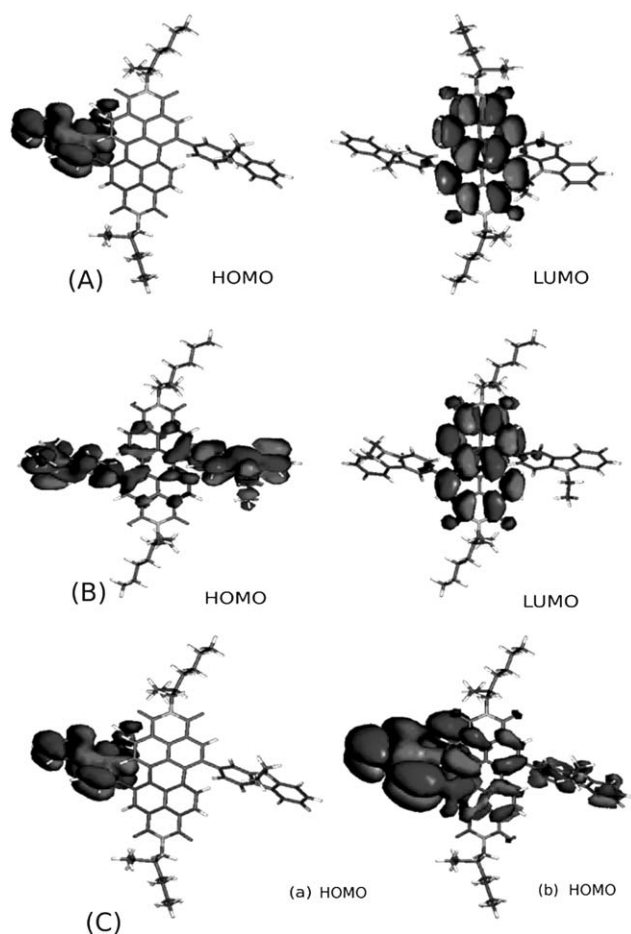


Fig. 7 FMOs obtained from quantum chemistry analysis. Comparison of HOMO and LUMO orbitals for the molecules **2** (A) and **3** (B) as obtained from DFT calculations. (C) HOMO orbitals for molecule **2** at two different isosurface values.

Table 5 HOMO, LUMO and various angles of **2** and **3** from DFT calculations^a

Compound	$E_{\text{HOMO}}/\text{eV}$	$E_{\text{LUMO}}/\text{eV}$	E_g/eV	α°	β_1°	β_2°
2	-5.77	-3.36	2.41	20.66	56.77	61.73
3	-5.61	-3.28	2.33	19.52	57.69	56.03

^a E_g – Band gap. (α) – Perylene core twisting (dihedral) angle. (β_1, β_2) – torsional angles of carbazoles with perylene core.

attachment at the bay position of perylene bisimides. Calculated band-gaps for these molecules were found to be 2.41 eV and 2.33 eV respectively for species **2** and **3**. The band gap energies calculated seem to deviate by a small factor from the experimentally determined ones, but this is owing to the fact that the quantum chemistry calculations are performed at vacuum and the crystalline nature of the model. Another important feature to address here is the twisting of the perylene core (α) and the twisted bay substitution (β) of carbazoles around the perylene bisimide as these parameters play a significant role in defining the properties of these materials. Fig. 8 demonstrates different twisting angles in these molecules and their values are described

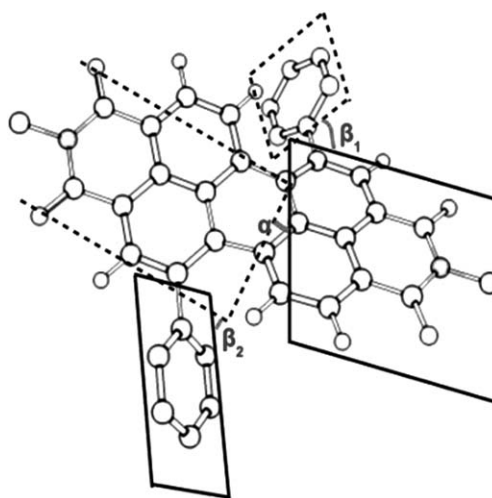


Fig. 8 Schematic to demonstrate different twist angles in carbazole substituted perylene bisimides. For clarity instead of carbazolyl groups only phenyl groups are shown.

in Table 5. The calculations imply that the dihedral angle (α) for both **2** and **3** is $\sim 20^\circ$ as reported with perylenes before.⁴⁴ As far as the torsional angle (β) is concerned, it is seen that **3** possesses a twisting angle of $\sim 57^\circ$ (both β_1 and β_2) and that of **2** is found to be $\sim 56^\circ$ (β_1) and $\sim 62^\circ$ (β_2). Thus here, it can be seen that there is a considerable difference in β angles between **2** and **3**. It is clearly noticeable that β_1 for **2** and **3** are similar, but β_2 shows a deviation by $\sim 6^\circ$. This is also quite visible in their FMOs, as in **2**, for which it can be seen that the electron cloud is much concentrated on one of the carbazoles where it makes more inclination with the perylene core. This might be due to the existence of strong twist between two chromophoric sub units that in turn is limiting the spatial orbital overlap.⁴⁷ This could be the reason for the different optical and complementary charge transporting properties of these regioisomers.

3. Experimental

3.1. Materials and methods

All chemicals and solvents are of reagent grade and were used as received unless otherwise indicated. Dichloromethane and THF were purified by standard distillation procedures prior to use. Nuclear magnetic resonance spectra were obtained in deuterated chloroform with a Varian Unity Inova spectrometer operating at 300 and 75.5 MHz for ^1H and ^{13}C nuclei respectively. All the data are given as chemical shifts δ (ppm) downfield from TMS. IR-spectroscopy measurements were performed on a Perkin Elmer Spectrum GX spectrophotometer, using KBr pellets. The absorbance and fluorescence spectra were recorded on a Shimadzu 3101 PC spectrophotometer and an RF-5301PC Shimadzu spectrofluorometer, respectively. Mass spectra were obtained on a Waters Micromass ZQ mass spectrometer. The molecular weights of the target molecules were determined by MALDI-TOF using a Shimadzu Biotech Axima Performance system and 2,5-dihydroxybenzoic acid (DHB) was used as the matrix under reflector mode of operation. Differential scanning calorimetry measurements were performed on a Perkin Elmer

Pyrus Diamond DSC apparatus at a heating/cooling rate of 10 °C min⁻¹ under nitrogen atmosphere and thermogravimetric analysis was executed on a TA Instruments Q100 under nitrogen atmosphere at a heating rate of 20 °C min⁻¹. Cyclic voltammetry measurements were carried out with a glassy carbon working electrode in a three-electrode cell using a μ -Autolab Type III (EcoChemie, Netherlands) potentiostat.

The ionization potentials (I_p) were measured by photoelectron spectroscopy in air. The materials were dissolved in THF and coated onto Al plates pre-coated with ~0.5 μ m thick methyl methacrylate and methacrylic acid copolymer (MKM) adhesive layer. The function of the MKM layer is not only to improve adhesion, but also to eliminate the electron photoemission from the Al layer. In addition, this layer is conductive enough to avoid charge accumulation on it during the measurements. The thickness of the layers was 0.5–1 μ m.

Charge drift mobilities of the neat materials or molecular mixtures with a polymer host bisphenol Z polycarbonate (PC-Z) were estimated by the xerographic time-of-flight method. The samples for the measurements were prepared by casting the solutions of the compounds or solutions of the mixtures of these compounds with binder materials PC-Z at mass proportion 1 : 1 in THF. The substrates were glass plates with a conductive SnO₂ layer or polyester film with Al layer. After coating the samples were heated at 80 °C for 1 h. Thus the transporting layers of the samples were prepared. In some cases, in order to avoid crystallization, the layers were dried at room temperature for several hours. The thickness of the transporting layer varied in the range of 1–7 μ m. Electron drift mobility (μ) was measured in the xerographic mode. The electric field was created by negative corona charging. The charge carriers were generated at the layer surface by illumination with pulses of nitrogen laser (pulse duration was 1 ns, wavelength 337 nm). The layer surface potential decrease as a result of pulse illumination was up to 1–5% of initial potential before illumination. The capacitance probe connected to the wide frequency band electrometer measured the speed of the surface potential decrease dU/dt . The transit time t_t for the samples with the transporting material was determined by the kink on the curve of the dU/dt transient in linear scale. In other cases, the dispersion of the transient current was larger and log–log scale was used. The drift mobility was calculated by using the formula $\mu = d^2/U_0 t_t$, where d is the layer thickness, and U_0 the surface potential at the moment of illumination.

DFT calculations were as implemented in the *Gamess US* package. Compounds were first geometry optimised using a semi-empirical PM6 basis set as implemented in *MOPAC* and these PM6 optimized geometries were further subjected to complete geometry optimization using DFT calculations at the basis B3LYP/6-311G*. Optimized structures were then used to perform single point energy calculations at B3LYP/6-311++G** basis set.

3.2. General procedure for the synthesis of 1,7-dibromo perylene bisimides

3,4,9,10-perylenetetracarboxylic anhydride (5 g, 12.7 mmol) was suspended in 100 mL of concentrated sulfuric acid and 250 mg of iodine was added to it. It was heated at 80 °C for 45 min followed

by dropwise addition of 8 mL of bromine for a period of 30 min and stirred for 24 h. The reaction mixture was cooled to room temperature and water was added into it. The precipitated product was filtered, washed with acetone and dried in vacuum. Thus obtained bromo substituted perylene dianhydride (2 g, 3.65 mmol) was suspended in 40 mL of *N*-methylpyrrolidone and mixed with 20 mL of glacial acetic acid. It was heated at 60 °C for 20 min and 2-ethylhexylamine (1.5 mL, 9.12 mmol) or *n*-dodecylamine (2.1 mL, 9.12 mmol) was added. The temperature was raised to 120 °C and stirring was continued for 12 h under nitrogen atmosphere. The mixture was poured into 300 mL of water and the precipitated product was filtered. It was washed with methanol, subjected to column chromatography (silica gel, eluent hexane–ethyl acetate, 8 : 2) and the desired product was isolated.

1,7-dibromo *N,N'*-2-ethylhexyl perylene bisimide (5). Yield = 52%, red solid. ¹H NMR (300 MHz, CDCl₃, δ ppm): 9.48 (d, J = 2.8 Hz, 2H), 8.91 (s, 2H), 8.70 (d, J = 2.7 Hz, 2H), 4.23–4.11 (m, 4H, NCH₂), 2.03–1.91 (m, 2H, CH), 1.47–1.28 (m, 16H, CH₂), 1–0.91 (m, 12H, CH₃); MS (EI) m/z = 773 (M⁺).

1,7-dibromo *N,N'*-dodecyl perylene bisimide (6). Yield = 45%, red solid. ¹H NMR (300 MHz, CDCl₃, δ ppm): 9.49 (d, J = 2.7 Hz, 2H), 8.91 (s, 2H), 8.71 (d, J = 2.7 Hz, 2H), 4.27–4.18 (m, 4H, NCH₂), 1.78 (b, 4H, CH₂), 1.44 (b, 4H, CH₂), 1.29 (b, 32H, CH₂), 0.9 (t, J = 4.4 Hz, 6H, CH₃); MS (EI) m/z = 885 (M⁺).

3.3. General procedure for Suzuki–Miyaura reactions

1,7-dibromo *N,N'*-2-ethylhexyl perylene bisimide (300 mg, 0.39 mmol) or 1,7-dibromo *N,N'*-dodecyl perylene bisimide (300 mg, 0.34 mmol) and the corresponding mono boronic acid or esters (2.2 molar equiv.) were dissolved in a solvent mixture of 15 mL of THF and 2 mL of water. Powdered potassium hydroxide (3.3 molar equiv.) was added and the reaction mixture was purged with nitrogen for 10 min. Then the reaction vessel was degassed. Bis(triphenylphosphine) palladium(II) dichloride (0.03 molar equiv.) was added into it and stirred for 8–12 h at 80 °C under nitrogen. After completion, the reaction mixture was diluted with water and extracted with ethyl acetate. The organic layer was dried over sodium sulfate and evaporated. The crude product was purified by column chromatography using silica gel as stationary phase and hexane–ethyl acetate mixture (97 : 3 for **1**; 95 : 5 for **2&3**; 9 : 1 for **4**) as eluent.

1,7-bis[4-(diphenylamino)phenyl] *N,N'*-2-ethylhexyl perylene bisimide (1). Yield = 24%; black solid. ¹H NMR (300 MHz, CDCl₃, δ ppm): 8.63 (s, 2H), 8.24 (d, J = 2.8 Hz, 2H), 8.06 (d, J = 2.7 Hz, 2H), 7.42–7.34 (m, 12H), 7.24–7.1 (m, 16H), 4.26–4.1 (m, 4H, NCH₂), 1.99–1.94 (m, 2H, CH), 1.47–1.31 (m, 16H, CH₂), 0.99–0.92 (m, 12H, CH₃). ¹³C NMR (75.5 MHz, CDCl₃, δ ppm): 164.1, 148.7, 147.4, 141.0, 135.6, 135.4, 135.3, 132.5, 130.2, 129.8, 129.6, 129.3, 125.4, 124.0, 123.9, 122.3, 122.0, 44.5, 38.2, 31.0, 29.0, 24.3, 23.3, 14.4, 10.9. IR (KBr), ν /cm⁻¹: (arene C–H) 3061, 3034; (aliphatic C–H) 2955, 2924, 2856; (imide C=O) 1698; (Ar C=C) 1659, 1586; (imide C–N) 1326, 1270. Anal. Calc. for C₇₆H₆₈N₄O₄: C, 82.88; H, 6.22; N, 5.09; O, 5.81%. Found: C,

82.39; H 6.44; N, 4.85%. MS (MALDI-TOF) m/z = 1100.29 (exact mass = 1100).

1,7-bis(9-ethyl-2-carbazolyl) N,N' -2-ethylhexyl perylene bisimide (2). Yield = 41%; black solid. ^1H NMR (300 MHz, CDCl_3 , δ ppm): 8.64–8.51 (m, 2H), 8.23–7.96 (m, 7H), 7.74–7.46 (m, 7H), 7.34–7.02 (m, 4H), 4.83–4.25 (m, 8H, NCH_2), 1.98–1.94 (m, 2H, CH), 1.39 (b, 16H, CH_2), 1.28 (b, 6H, CH_3), 1.01–0.89 (m, 12H, CH_3). ^{13}C NMR (75.5 MHz, CDCl_3 , δ ppm): 164.0, 163.7, 141.9, 140.9, 139.4, 135.5, 131.8, 130.4, 128.9, 126.5, 125.8, 122.6, 122.1, 121.7, 119.9, 119.6, 109.0, 44.6, 38.4, 31.0, 30.5, 29.9, 29.7, 29.0, 25.0, 24.4, 23.3, 14.4, 10.9. IR (KBr), ν/cm^{-1} : (arene C–H) 3051; (aliphatic C–H) 2955, 2924, 2855; (imide C=O) 1695; (Ar C=C) 1652, 1584; (imide C–N) 1326, 1259. Anal. Calc. for $\text{C}_{68}\text{H}_{64}\text{N}_4\text{O}_4$: C, 81.57; H, 6.44; N, 5.60; O, 6.39%. Found: C, 81.68; H, 7.21; N, 5.03%. MS (MALDI-TOF) m/z = 1000.30 (exact mass = 1000).

1,7-bis(9-ethyl-3-carbazolyl) N,N' -2-ethylhexyl perylene bisimide (3). Yield = 55%; black solid. ^1H NMR (300 MHz, CDCl_3 , δ ppm): 8.69 (s, 2H), 8.33 (b, 4H), 8.01 (d, J = 2.8 Hz, 2H), 7.79–7.73 (m, 2H), 7.59–7.51 (m, 5H), 7.38 (b, 5H), 4.49–4.42 (m, 4H, NCH_2), 4.27–4.12 (m, 4H, NCH_2), 1.99 (b, 2H, CH), 1.55 (t, J = 4.8 Hz, 6H, CH_3), 1.49–1.28 (m, 16H, CH_2), 0.99–0.89 (m, 12H, CH_3). ^{13}C NMR (75.5 MHz, CDCl_3 , δ ppm): 164.1, 163.8, 141.9, 140.6, 140.1, 135.9, 134.9, 132.7, 129.8, 129.3, 128.9, 127.1, 126.9, 126.5, 121.9, 121.5, 109.1, 44.6, 38.3, 38.1, 31.1, 29.1, 24.4, 23.3, 14.4, 14.2, 10.9. IR (KBr), ν/cm^{-1} : (arene C–H) 3050; (aliphatic C–H) 2954, 2925, 2856; (imide C=O) 1695; (Ar C=C) 1656, 1585; (imide C–N) 1327, 1256. Anal. Calc. for $\text{C}_{68}\text{H}_{64}\text{N}_4\text{O}_4$: C, 81.57; H, 6.44; N, 5.60; O, 6.39%. Found: C, 81.46; H 6.75; N, 5.35%. MS (EI) m/z = 1001(M^+). MS (MALDI-TOF) m/z = 1000.40 (exact mass = 1000).

1,7-bis(9-ethyl-3-carbazolyl) N,N' -dodecyl perylene bisimide (4). Yield = 32%; black solid. ^1H NMR (300 MHz, CDCl_3 , δ ppm): 8.54–8.47 (m, 4H), 8.2 (b, 2H), 8.02 (b, 2H), 7.51 (b, 8H), 7.39 (b, 2H), 7.24 (b, 2H), 4.42–4.3 (m, 8H, NCH_2), 1.82 (b, 4H, CH_2), 1.52–1.29 (m, 42H, CH_2 , CH_3), 0.93–0.89 (m, 6H, CH_3). ^{13}C NMR (75.5 MHz, CDCl_3 , δ ppm): 163.7, 163.4, 141.9, 140.6, 140, 136.6, 135.8, 135, 132.7, 132, 129.9, 129.3, 128.9, 127.1, 126.9, 126.5, 123.2, 122, 121.5, 119.8, 109.1, 100.2, 72.5, 62.1, 41, 38, 32.1, 29.9, 29.8, 29.7, 29.6, 28.4, 27.4, 22.9, 14.4, 14.2. IR (KBr), ν/cm^{-1} : (arene C–H) 3051; (aliphatic C–H) 2922, 2851; (imide C=O) 1694; (Ar C=C) 1655, 1586; (imide C–N) 1331, 1256. Anal. Calc. for $\text{C}_{76}\text{H}_{80}\text{N}_4\text{O}_4$: C, 81.98; H, 7.24; N, 5.03; O, 5.75%. Found: C, 81.78; H 7.25; N, 4.86%. MS (MALDI-TOF) m/z = 1112.18 (exact mass = 1112).

4. Conclusions

In summary, we have designed and synthesized a series of functional multichromophoric (donor–acceptor–donor) molecular materials based on bay substituted perylene bisimide and examined their properties. They absorb well in the visible–near IR region with efficient photo-induced intramolecular charge transfer. It is found that bay substituents influence the optical properties and the drift mobility of charge carriers can be tuned by the proper substitution of electron donors at the bay region.

Triphenylamino substituted perylene bisimides exhibit excellent n-type characteristics with good air stability whereas bay carbazolyl substituted perylene bisimide derivatives can transport both electrons and holes in ambient conditions. Changing the linking topology of carbazolyl moieties to the core of perylene bisimides has furnished materials with complementary semi-conducting properties. These new electro-active multichromophoric organic semiconductors with wide absorption window, excellent photo-induced intramolecular charge transfer and efficient charge carrier mobilities may find application in various organic electronic and optoelectronic devices.

Acknowledgements

This research work was supported by FP-7 PEOPLE PROGRAMME, Marie Curie Actions – ITN Grant No. 215884. A. Swinarew is thanked for MALDI-TOF measurements. K. Kazalaukas is thanked for the measurements of fluorescence quantum yields. Asta Sakalyte and Jurate Simokaitiene are thanked for the TGA and DSC measurements.

References

- 1 Y. Shirota and H. Kageyama, *Chem. Rev.*, 2007, **107**, 953–1010.
- 2 A. W. Hains, Z. Liang, M. A. Woodhouse and B. A. Gregg, *Chem. Rev.*, 2010, **110**, 6689–6735.
- 3 A. Hagfeldt, G. Boschloo, L. Sun, L. Kloo and H. Pettersson, *Chem. Rev.*, 2010, **110**, 6595–6663.
- 4 C. D. Dimitrakopoulos and P. R. L. Malenfant, *Adv. Mater.*, 2002, **14**, 99–117.
- 5 M. E. Roberts, A. N. Sokolov and Z. Bao, *J. Mater. Chem.*, 2009, **19**, 3351–3363.
- 6 J. E. Anthony, A. Facchetti, M. Heeney, S. R. Marder and X. Zhan, *Adv. Mater.*, 2010, **22**, 3876–3892.
- 7 R. Schmidt, J. H. Oh, Y. Sun, M. Deppisch, A. Krause, K. Radacki, H. Braunschweig, M. Konemann, P. Erk, Z. Bao and F. Wurthner, *J. Am. Chem. Soc.*, 2009, **131**, 6215–6228.
- 8 B. A. Jones, A. Facchetti, M. R. Wasielewski and T. J. Marks, *J. Am. Chem. Soc.*, 2007, **129**, 15259–15278.
- 9 A. P. Kulkarni, C. J. Tonzola, A. Babel and S. A. Jenekhe, *Chem. Mater.*, 2004, **16**, 4556–4573.
- 10 D. M. de Leeuw, M. M. J. Simenon, A. R. Brown and R. E. F. Einerhand, *Synth. Met.*, 1997, **87**, 53–59.
- 11 Y. Wen and Y. Liu, *Adv. Mater.*, 2010, **22**, 1–15.
- 12 C. R. Newman, C. D. Frisbie, D. A. S. Filho, J. Bredas, P. C. Ewbank and K. R. Mann, *Chem. Mater.*, 2004, **16**, 4436–4451.
- 13 F. Wurthner, *Chem. Commun.*, 2004, 1564–1579.
- 14 H. Langhals, *Helv. Chim. Acta*, 2005, **88**, 1309–1343.
- 15 Y. Avlasevich, C. Li and K. Mullen, *J. Mater. Chem.*, 2010, **20**, 3814–3826.
- 16 F. Wurthner, *Pure Appl. Chem.*, 2006, **78**, 2341–2349.
- 17 H. Tsuji, C. Mitsui, Y. Sato and E. Nakamura, *Adv. Mater.*, 2009, **21**, 3776–3779.
- 18 Y. L. Liao, C. Y. Lin, Y. H. Liu, K. T. Wong, W. Y. Hung and W. J. Chen, *Chem. Commun.*, 2007, 1831–1833.
- 19 W. Y. Hung, T. C. Wang, H. C. Chiu, H. F. Chen and K. T. Wong, *Phys. Chem. Chem. Phys.*, 2010, **12**, 10685–10687.
- 20 C. Liu, Z. Liu, H. T. Lemke, H. N. Tsao, R. C. G. Naber, Y. Li, K. Banger, K. Mullen, M. M. Nielsen and H. Sirringhaus, *Chem. Mater.*, 2010, **22**, 2120–2124.
- 21 P. Stroehriegl and J. V. Grazulevicius, *Adv. Mater.*, 2002, **14**, 1439–1452.
- 22 J. V. Grazulevicius, P. Stroehriegl, J. Pieliowski and K. Pieliowski, *Prog. Polym. Sci.*, 2003, **28**, 1297–1353.
- 23 S. Beaupre, P. T. Boudreault and M. Leclerc, *Adv. Mater.*, 2010, **22**, E6–E27.
- 24 J.-F. Morin, M. Leclerc, D. Ades and A. Siove, *Macromol. Rapid Commun.*, 2005, **26**, 761–778.
- 25 A. Tomkeviciene, J. V. Grazulevicius, K. Kazalaukas, A. Gruodis, S. Jursenas, T.-H. Ke and C.-C. Wu, *J. Phys. Chem. C*, 2011, **115**, 4887–4897.

- 26 N. Blouin and M. Leclerc, *Acc. Chem. Res.*, 2008, **41**, 1110–1119.
- 27 A. Tomkeviciene, J. V. Grazulevicius and V. Jankauskas, *Chem. Lett.*, 2008, **37**, 344–345.
- 28 A. W. Freeman, M. Urvoy and M. E. Criswell, *J. Org. Chem.*, 2005, **70**, 5014–5019.
- 29 V. Percec, M. Obata, J. G. Rudick, B. B. De, M. Glodde, T. K. Bera, S. N. Magonov, V. S. K. Balagurusamy and P. A. Heiney, *J. Polym. Sci., Part A: Polym. Chem.*, 2002, **40**, 3509–3533.
- 30 W. Tang, T. Lin, L. Ke and Z. Chen, *J. Polym. Sci., Part A: Polym. Chem.*, 2008, **46**, 7725–7738.
- 31 Z. Li, Z. Li, C. Di, Z. Zhu, Q. Li, Q. Zeng, K. Zhang, Y. Liu, C. Ye and J. Qin, *Macromolecules*, 2006, **39**, 6951–6961.
- 32 M. Tavasli, S. Bettington, M. R. Bryce, A. S. Batsanov and A. P. Monkman, *Synthesis*, 2005, **10**, 1619–1624.
- 33 V. Sivamurugan, K. Kazlauskas, S. Jursenas, A. Gruodis, J. Simokaitiene, J. V. Grazulevicius and S. Valiyaveetil, *J. Phys. Chem. B*, 2010, **114**, 1782–1789.
- 34 S. Vajiravelu, R. Lygaitis, J. V. Grazulevicius, V. Gaidelis, V. Jankauskas and S. Valiyaveetil, *J. Mater. Chem.*, 2009, **19**, 4268–4275.
- 35 T. Edvinsson, C. Li, N. G. Pschirer, J. Schoneboom, F. Eickemeyer, R. Sens, G. Boschloo, A. Herrmann, K. Mullen and A. Hagfeldt, *J. Phys. Chem. C*, 2007, **111**, 15137–15140.
- 36 P. Osswald, D. Leusser, D. Stalke and F. Wurthner, *Angew. Chem., Int. Ed.*, 2005, **44**, 250–253.
- 37 M. L. Tang, A. D. Reichardt, P. Wei and Z. Bao, *J. Am. Chem. Soc.*, 2009, **131**, 5264–5273.
- 38 J. Li, F. Dierschke, J. Wu, A. C. Grimsade and K. Mullen, *J. Mater. Chem.*, 2006, **16**, 96–100.
- 39 G. Gritzner, *Pure Appl. Chem.*, 1990, **62**, 1839–1858.
- 40 S. Chen, Y. Liu, W. Qiu, X. Sun, Y. Ma and D. Zhu, *Chem. Mater.*, 2005, **17**, 2208–2215.
- 41 J. Qu, N. G. Pschirer, D. Liu, A. Stefan, F. C. D. Schryver and K. Mullen, *Chem.–Eur. J.*, 2004, **10**, 528–537.
- 42 P. M. Borsenberger, L. Pautmeier and H. Bassler, *J. Chem. Phys.*, 1991, **94**, 5447–5454.
- 43 H. Bassler, *Int. J. Mod. Phys. B*, 1994, **8**, 847–854.
- 44 Y. Geng, J. Wang, S. Wu, H. Li, F. Yu, G. Yang, H. Gao and Z. Su, *J. Mater. Chem.*, 2011, **21**, 134–143.
- 45 M. W. Schmidt, K. K. Baldrige, J. A. Boatz, S. T. Elbert, M. S. Gordon, J. H. Jensen, S. Koseki, N. Matsunaga, K. A. Nguyen, S. Su, T. L. Windus, M. Dupuis and J. A. Montgomery, *J. Comput. Chem.*, 1993, **14**, 1347–1363.
- 46 J. J. P. Stewart, *J. Mol. Model.*, 2007, **13**, 1173–1213.
- 47 C. Li, J. Schoneboom, Z. Liu, N. G. Pschirer, P. Erk, A. Herrmann and K. Mullen, *Chem.–Eur. J.*, 2009, **15**, 878–884.